JCAMECH

Vol. 50, No. 1, June 2019, pp 157-164
DOI: 10.22059/JCAMECH.2019.281000.391

Dynamics analysis of microparticles in inertial microfluidics for biomedical applications

E. Rohani Rad [a]∗ and M.R. Farajpour [b]

[a] *Faculty of Health and Medical Sciences, Adelaide Medical School, University of Adelaide, Adelaide, Australia*
[b] *Borjavaran Center of Applied Science and Technology, University of Applied Science and Technology, Tehran, Iran*

ARTICLE INFO

Article history:
Received: 09 April 2019
Accepted: 13 May 2019

Keywords:
Inertial microfluidics
Particle separation
Particle sorting
Intrinsic forces

ABSTRACT

Inertial microfluidics-based devices have recently attracted much interest and attention due to their simple structure, high throughput, fast processing and low cost. They have been utilised in a wide range of applications in microtechnology, especially for sorting and separating microparticles. This novel class of microfluidics-based devices works based on intrinsic forces, which cause microparticles to migrate laterally and locate at their equilibrium positions. In this article, a comprehensive theoretical formulation is presented for the dynamics of ultrasmall particles in microfluidics-based devices. Explicit expressions are presented for various important forces, which act on a microparticle, such as drag, Magnus, Saffman and wall-induced forces. In addition, the drag coefficient, diffusion phenomenon and Peclet number are formulated. Finally, the influences of particle size, as a crucial parameter, on various intrinsic forces including drag, Magnus and Saffman forces as well as the wall-induced force, are investigated. It is found that the drag, wall-induced and Saffman forces have an important role to play in the dynamics of microparticles in inertial microfluidics while the effects of Magnus force and diffusion can be ignored in most applications.

1. Introduction

Microelectromechanical and nanoelectromechanical devices involving small-scale resonators [1, 2], generators [3] and sensors [4-6] have been widely manufactured and analysed in recent years due to their fascinating functions and features. Various structural components (ultrasmall beams, plates and channels) [7-14] have been utilised in their manufacturing process. The mechanics of these components [15-19] has been an interesting topic for researchers and scientist all over the world as well [20-24]. Microfluidics-based devices are a novel class of microelectromechanical systems, which are used to control and manipulate fluid and particle behaviour at microscale levels [25, 26]. These ultrasmall devices have a wide range of applications from biomedical systems [27, 28] to the synthesis of polymeric ultrasmall particles. Compared to traditional tools for manipulating and controlling fluids and particles, it has a number of advantages including reduced process time, less fabrication cost, small size, being portable, high precision and less maintenance cost [26]. Moreover, microfluidics-based devices have the potential to be connected to smart phones [29]. In this way, for instance, there is no need for a laboratory and extra equipment to see the results of a biomedical test.

Generally, there are two important classes of microfluidics-based devices: 1) active, and 2) passive. In the first class (i.e. active devices), the device operates using an external applied force such as electrical and magnetic forces whereas in the second class, there is no external force, and the device works based on intrinsic forces. Among passive microfluidics-based devices, inertial microfluidics has attracted much attention owing to their advantages such as having a simple structure, high throughput, fast processing and low cost [26, 27]. This type of microscale systems plays a crucial role in focusing and separating particles and fluids at the scale of micrometres. In comparison with traditional microfluidic devices, where Reynolds number is less than one, meaning that the fluid velocity is very low and viscosity is large, inertial microfluidics has an intermediate Reynolds number. Inertial microfluidic devices can be used in biomechanical and biomedical applications such as detecting and diagnosing malaria, detaching circulating tumour cells and extracting blood plasma.

* Corresponding author. E-mail addresses: elaheh.rohanirad@student.adelaide.edu.au (E. Rohani Rad). Phone: +61404821813

Inertial migration and secondary flow are the basis of inertial microfluidics. When particles flow in a straight channel, inertial lift forces cause particles to migrate laterally to the equilibrium position. There are two main kinds of inertial effects that act in an opposite manner. 1) Saffman and shear gradient forces, which cause particles to move away from the centre, and 2) wall-induced force, which repels particles away from the wall due to their interaction with the channel wall. These two inertial forces are balanced with each other, leading particles to the equilibrium position [30, 31]. The secondary flow, which is induced by the pressure gradient due to the fluid momentum difference between the centre and wall, is observed in straight channels as well as curved ones. The centre of the channel has a higher velocity compared to the regions near the wall. Therefore, when particles flow through the curved channel, they go towards the channel and then recirculates back, forming two different streams in the cross-sectional plane of the channel (Dean vortex) [32, 33]. Moreover, dean drag force has been added to inertial lift forces, determining the equilibrium position. The ratio of the inertial lift force to dean drag force is important in differentiating and separating particles based on their size (see Fig. 1). In a straight channel, the inertial lift force is generated as particles flow in the fluid, leading to the lateral migration. In a curved channel, inertial lift forces together with dean drag force are generated, determining the final equilibrium position. Curved channels are able to separate particles based on their size while straight channels are not reasonable for this purpose.

There are nonlinear forces in inertial microfluidics that have been used to manipulate microparticles. These forces include but not limited to viscous drag, diffusion, Magnus, Saffman and wall-induced forces. When a particle/object moves in fluid, an external force acts on the particle, causing the viscous drag force. Random movements of ultrasmall particles in fluid create diffusion force. There is low diffusion process if the viscosity of fluid is high or particles are large. Magnus force is associated with a rotating object in fluid. It is due to pressure difference because of the spinning of the object in fluid. Furthermore, because of channel walls, a velocity gradient is generated, causing a lift force (Saffman force). Finally, the wall-induced force, which acts on particles near boundaries, together with Magnus and Saffman forces, cause the lateral migration of particles. In this paper, all of these important forces are formulated and discussed in detail. This is a comprehensive paper which deals with a high number of intrinsic forces in inertial microfluidics-based devices. In addition to mathematical formulation of intrinsic forces, the influences of particle size on the drag force, drag coefficient, particle Reynolds number, diffusion coefficient and Peclet number as well as Magnus, Saffman and wall-induced forces are examined and discussed.

2. Drag force

When particles move in a fluid, a force is required to carry the fluid molecules away from the path of particles. This force is technically called viscous drag force. Let us take into account a particle of a spherical shape which moves in a fluid. In this case, the drag force (F_D) can be expressed as [34]

$$F_D = c_D S = \frac{\pi}{4} c_D d_P^2, \tag{1}$$

where c_D, S, and d_P stand for the darg coefficient, particle cross-sectional area and diameter, respectively. c_D depends on the particle Reynolds number (Re_P), which is defined by

$$\mathrm{Re}_P = \frac{\rho_f d_P V_r}{\mu_f}. \tag{2}$$

Here ρ_f, μ_f and V_r are, respectively, the fluid density, fluid viscosity and the relative speed of the particle with respect to the fluid. The influences of being scale-dependent are neglected in this force analysis. The scale influences are usually captured for nanoscale structures [35-42].

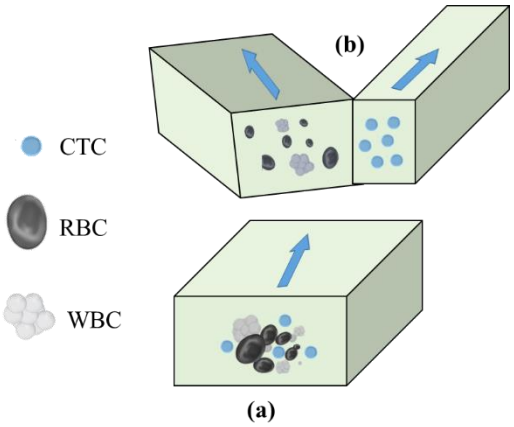

Fig. 1. (a) Inlet and (b) outlet of an inertial microfluidics-based device for CTC separation.

There are several ranges of Reynolds number for determining the drag coefficient, and then consequently for obtaining the drag force as follows:

1) $10^{-4} < \mathrm{Re}_P < 0.2$:

$$c_D = 12\frac{\mu_f V_r}{d_P}, \tag{3}$$

and

$$F_D = 3\pi\mu_f V_r d_P, \tag{4}$$

The drag force in this case, is commonly known as the Stokes drag. Stokes drag happens if the relative speed of particles to fluid is sufficiently small. The second range is [34]

2) $0.2 < \mathrm{Re}_P < 500 \sim 1000$:

$$c_D = 12\frac{\mu_f V_r}{d_P}\left[1 + 0.15\left(\mathrm{Re}_P\right)^{0.687}\right], \tag{5}$$

and

$$F_D = 3\pi\left[1 + 0.15\left(\mathrm{Re}_P\right)^{0.687}\right]\mu_f V_r d_P, \tag{6}$$

3) $500 \sim 1000 < \mathrm{Re}_P < 2\times10^5$:

$$c_D = 0.22\rho_f\left(V_r\right)^2, \tag{7}$$

and

$$F_D = 0.055\pi\rho_f\left(V_r\right)^2 d_P^2. \tag{8}$$

In inertial microfluidics-based channels, there are two drag force components: 1) mainstream drag force, and 2) secondary flow drag force. The former is caused by the movement of particles along the direction of the channel whereas the latter is induced due to the secondary flow of particles. The mainstream drag force acts on the particle along the channel direction while the secondary flow darg force exists in the cross-sectional plane. It should be noticed that in inertial microfluidics, we have intermediate Reynolds numbers (i.e. $\sim 1 < \mathrm{Re}_P < \sim 100$) for the main stream, and thus the corresponding drag coefficient and force are obtained from Eqs. (5) and (6), respectively.

3. Diffusion force

The diffusion force, which acts on particles suspended in a fluid, is caused by the Brownian motion. Due to the frequent collision between suspended particles and fluid molecules, random

motions are observed, which are known as Brownian motions. Based on the Einstein-Smoluchowski relation, we have [43]

$$\left\langle r_{diff}^2 \right\rangle = 6c_{diff}t. \tag{9}$$

Here r_{diff}, c_{diff} and t denote the mean diffusion distance, diffusion coefficient and time, respectively. r_{diff} represents the mean distance which particles diffuse inside a fluid. Using the Stokes-Einstein assumption, c_{diff} can be written as

$$c_{diff} = \frac{kT}{3\pi d_p \mu_f}, \tag{10}$$

where k and T stand for Boltzmann's coefficient and absolute temperature, respectively. Boltzmann's coefficient is 1.3806485×10^{-23} J/K. To compare advection (main flow) to diffusion, a dimensionless number is given by

$$\mathrm{Pe} = \frac{\text{advection rate}}{\text{diffusion rate}} = \frac{V_f L_c}{c_{diff}}, \tag{11}$$

in which Pe, V_f and L_c are the Peclet number, fluid velocity and channel characteristic length, respectively [44]. When the Peclet number is small, the diffusion has an important effect on the motion of particles. In inertial microfluidics-based devices, the Peclet number is large, meaning that the effect of diffusion can be neglected.

4. Magnus force

When a particle rotates with angular speed $\vec{\omega}_p$ inside a flowing fluid with speed $\vec{V}_f$, a lift force, which is known as Magnus force, is created (see Fig. 2). In fact, the fluid speed is lower near the point where the particle speed is in the opposite direction to that of the flow, and thus the pressure is higher (Bernoulli principle). This difference in the pressure results in the Magnus force. For a rotating spherical particle, one obtains [45]

$$\vec{F}_M = \frac{1}{8}\pi d_P^3 \rho_f \vec{V}_f \times \vec{\omega}_P, \tag{12}$$

in which $\vec{F}_M$ is the Magnus force. When the rotating spherical particle moves inside the fluid with speed $\vec{V}_P$, the Magnus force is determined as

$$\vec{F}_M = \frac{1}{8}\pi d_P^3 \rho_f \left(\vec{V}_f - \vec{V}_P\right) \times \vec{\omega}_P. \tag{13}$$

The above-stated relations are true for irrotational fluid flow with low Reynolds numbers. When there is a rotational flow field for the fluid, we have

$$\vec{F}_M = \frac{1}{8}\pi d_P^3 \rho_f \left(\vec{V}_f - \vec{V}_P\right) \times \vec{\omega}_R, \tag{14}$$

where

$$\vec{\omega}_R = \vec{\omega}_P - \frac{1}{2}\nabla \times \vec{V}_f, \tag{15}$$

in which $\vec{\omega}_R$ is the relative angular velocity.

5. Saffman force

In general, there are two wall effects in a microfluidic channel: 1) a fluid speed gradient (shear rate) induced by the wall, and 2) retardation of the particle motion due to the presence of the wall. The lateral lift force caused by the first wall effect is known as Saffman force. One of important phenomena in inertial microfluidics is inertial migration, in which all particles of one type migrate to a particular distance from the channel centre after a certain length. For instance, for a straight tube of average radius R, particles migrate to the distance $0.6R$ from the centre. It should be noticed that this phenomenon is greatly affected by all wall effects.

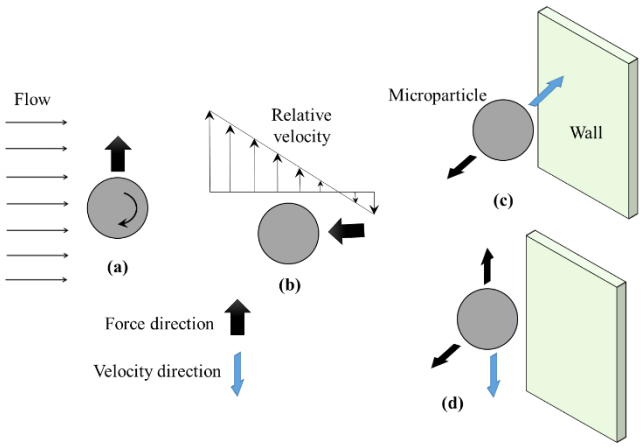

Fig. 2. (a) Magnus force, (b) Saffman force, (c) wall-induced force when the microparticle moves perpendicularly to the wall, and (d) wall-induced force when the microparticle moves parallel.

Let us take into account a particle in a simple shear flow, in which the shear rate is constant. Employing a matched asymptotic expansion technique, the transverse lift force on the particle of spherical shape is obtained as [46]

$$F_S = \frac{1}{4}K\mu_f d_P^2 V_r \left(\frac{c_g}{\upsilon}\right)^{\frac{1}{2}}, \tag{16}$$

where F_S, K, V_r, c_g and υ are, respectively, the Saffman force, a constant coefficient, relative speed, shear rate (velocity gradient) and kinetic viscosity. The constant K is commonly set to 81.2. The kinetic viscosity is related to the dynamic one as $\upsilon = \mu/\rho_f$. The direction of Saffman force is determined based on the magnitude of the relative speed (see Fig. 2). This force acts on the particle towards the place where the magnitude of V_r is larger. The relative speed of the particle can be expressed as

$$V_r = \left|\vec{V}_P - \vec{V}_f\right|, \tag{17}$$

where $\vec{V}_P$ and $\vec{V}_f$ denote the particle and fluid speeds, respectively.

6. Wall-induced force

As mentioned in the previous section, there are two distinct effects induced by the presence of the wall. The first one is the fluid velocity gradient, and the second effect is the retardation of particle motions. The later effect is studied in detail in this section. To remove the influences of the fluid velocity gradient (the first wall effect), it is assumed that the fluid is stagnant. Generally, to investigate the wall retardation effect, two overall cases are taken into consideration:

I) The motion of the particle is affected by a single wall. This assumption is true when the particle characteristic size is much smaller than that of the channel.

II) The particle motion is subject to all boundaries. In other words, the effects of all wall are important and cannot be neglected. This case happens when the particle characteristic size is in the range of the channel characteristic dimension.

First of all, it is assumed that the motion of particles in the stagnant fluid is under the effects of only one wall (i.e. case I).

There are two possibilities in this case: 1) the particle moves towards the wall, and 2) the particle moves parallel to the wall (Fig. 2). We will investigate these two possibilities in the following step by step. When the direction of the particle motion is perpendicular to the wall, a force is exerted on the particle in the opposite direction, retarding its motion (Fig. 2). It leads to an increase in the drag force. For a spherical particle approaching perpendicularly to a wall, the corrected drag force is [47]

$$\left(F_D\right)_{wall} = \frac{\pi}{4}\left(c_D\right)_{wall} d_P^2 = 4\pi\kappa d_P \mu_f V_r, \tag{18}$$

where

$$\left(c_D\right)_{wall} = \frac{16\kappa\mu_f V_r}{d_P}, \tag{19}$$

and

$$\kappa = \sinh(\varphi)\sum_{m=1}^{\infty}\frac{m(m+1)}{(2m-1)(2m+3)}\left[f(\varphi,m)-1\right], \tag{20}$$

in which f and φ are defined as

$$f(\varphi,m) = \frac{2\sinh\left((2m+1)\varphi\right)+(2m+1)\sinh(2\varphi)}{4\sinh^2\left((m+0.5)\varphi\right)-(2m+1)^2\sinh^2(\varphi)}, \tag{21}$$

$$f(\varphi,m) = \cosh^{-1}\left(2\ell_w/d_P\right), \tag{22}$$

where ℓ_w represents the distance between the particle centre and the wall.

In the case of an immersed spherical particle moving parallel to the wall, a lateral migration in the opposite direction of the wall is imposed on the particle. The speed of this migration is obtained as [48]

$$V_m = \frac{3}{64}\left(1-\frac{11}{32}h_w^2\right)V_s \mathrm{Re}_s, \tag{23}$$

where

$$\mathrm{Re}_s = \frac{\rho_f d_P V_s}{\mu_f},\quad h_w = \frac{\rho_f \ell_w V_s}{\mu_f}. \tag{24}$$

Here Re_s and V_s are, respectively, the sedimentation Reynolds number and velocity. Equation (23) is valid only for small values of h_w (i.e. $h_w \ll 1$). Taking into account this condition, one can further simplify the migration velocity as follows

$$V_m = \frac{3}{64}V_s \mathrm{Re}_s. \tag{25}$$

From the above relation, it is found that the migration velocity of particles is constant near the wall. Conducting experiment, it was indicated that Eq. (25) is valid up to Re_s=3. For large values of h_w (i.e. $h_w \gg 1$), we have

$$V_m = \frac{3}{16}\left(\frac{1}{h_w^2}+2.219\sqrt{\frac{1}{h_w^5}}\right)V_s \mathrm{Re}_s. \tag{26}$$

When the particle moves parallel to the wall, there are two different forces. The first force causes the particle to migrate laterally while the second one acts as a drag force against the sedimentation motion. Near the wall, this force is obtained by the following relation

$$F_D = 3\pi\mu_f d_P V_s\left(1+\frac{3}{8}\mathrm{Re}_s+\frac{9}{32}\frac{d_P}{\ell_w}\right), \quad for \quad \frac{d_P}{2\ell_w} \ll 1 \ll \frac{1}{\mathrm{Re}_s}. \tag{27}$$

In addition, for particles that moves at distances comparatively far from the wall, one obtains

$$F_D = 3\pi\mu_f d_P V_s\left(1+\frac{3}{8}\mathrm{Re}_s-0.095\frac{d_P}{\ell_w}\sqrt{\left(\frac{1}{\mathrm{Re}_s}\right)^3}\right), \quad for \quad \frac{d_P}{2\ell_w} \ll \frac{1}{\mathrm{Re}_s} \ll 1. \tag{28}$$

For the case II in which the particle is subject to the wall effects of all boundaries, the sedimentation motion is significantly influenced. This case is found when the spherical particle characteristic size such as its diameter has more or less the same order as that of microchannel. The drag force acting on a rigid spherical particle in a cylindrical tube full of stagnant fluid is determined as

$$F_D = 3\pi\kappa_{wall}\mu_f d_P V_s, \tag{29}$$

where κ_{wall} is a coefficient associated with geometrical properties, which is obtained as [44]

$$\kappa_{wall} = \left(1-2.014\lambda_b+2.089\left(\lambda_b\right)^3 -6.948\left(\lambda_b\right)^5-1.372\left(\lambda_b\right)^6\right)^{-1}, \tag{30}$$

in which λ_b indicates the blockage ratio, which is given by $\lambda_b = d_P/d_C$. Here d_C is the channel dimeter. It is worth mentioning that the blockage ratio (λ_b) must be less than 1 in order to avoid blockage.

7. Results and discussion

In the following, a comprehensive force analysis is conducted to compare and recognise which types of forces are dominant in an inertial microfluidics-based device. Let us consider a spherical rigid microparticle of diameter d_P in a microchannel with flowing fluid of density 1000 kg/m^3 and viscosity 8.90×10^{-4} Pa$\cdot$s. The value of the particle diameter varies from 5 to 75 micrometres. The fluid itself is supposed to be Newtonian and incompressible. These values are assumed for the particle and fluid throughout this section, unless otherwise stated.

Figure 3 is plotted to illustrate the influences of particle size on the drag force in an inertial microfluidics-based device. The relative speed between the microparticle and fluid is set to 1 m/s. It is found that as the diameter of the microparticle plays a crucial role in the drag force in an inertial microfluidics-based device. As the particle diameter increases, the drag force substantially increases. In addition, the drag coefficient for the microparticle, which moves in an inertial microfluidics-based device, is shown in Fig. 4. The value of the particle diameter varies from 5 to 75 micrometres. It is interesting that unlike the drag force, the drag coefficient substantially decreases when the particle size increases. The particle Reynolds number is also indicated in Fig. 5 to make sure it is in the common range in which inertial microfluidics-based devices operate. It should be noticed that the drag force

analysed here is the mainstream drag force, but not the one induced by the secondary flow.

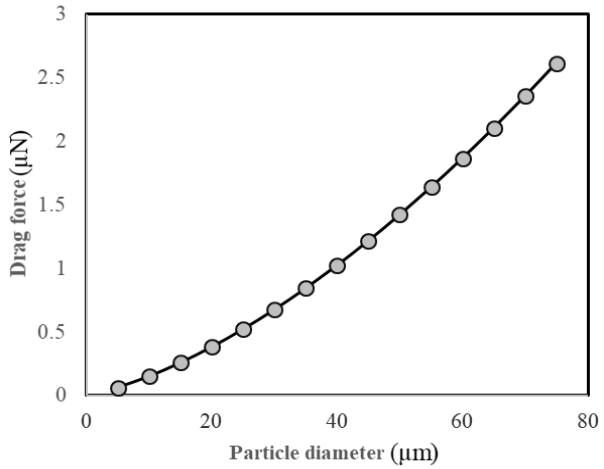

Fig. 3. Drag force acting on a microparticle in a microchannel versus the particle diameter.

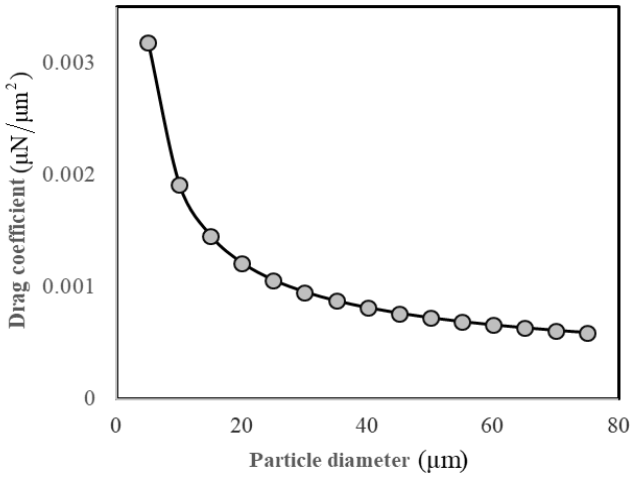

Fig. 4. Drag coefficient for a microparticle in a microchannel versus the particle diameter.

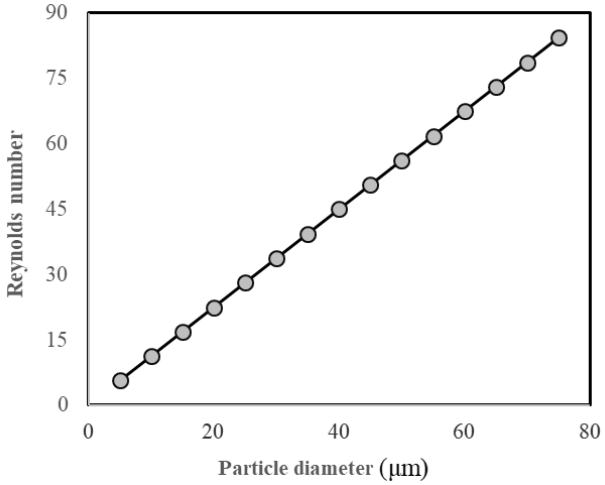

Fig. 5. Particle Reynolds number (Re_P) versus the particle diameter.

To investigate the influences of diffusion on microparticles in an inertial microfluidics-based device, Figs. 6 and 7 are plotted, showing the diffusion coefficient and Peclet number, respectively. The temperature inside the device is assumed to be 25 ^{0}C. Furthermore, the fluid velocity is set to 10 m/s. These figures are plotted for time t=1 s and channel dimeter L_C=300 micrometers. From Figs. 6 and 7, it is seen that the diffusion coefficient is very small whereas the Peclet number is very high. Therefore, from these results, it can be concluded that the effects of diffusion can be neglected in an inertial microfluidics-based device. In fact, when the Peclet number is very high, the ratio of advection to diffusion is large, and consequently diffusion is negligible compared to the mainstream flow.

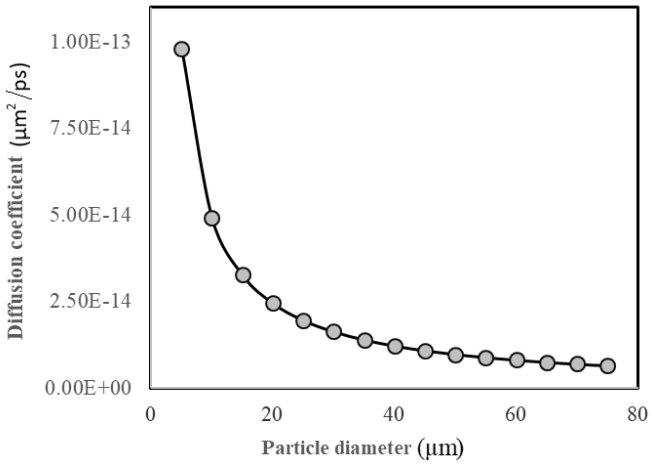

Fig. 6. Diffusion coefficient for a microparticle in a microchannel obtained via Stokes-Einstein relation.

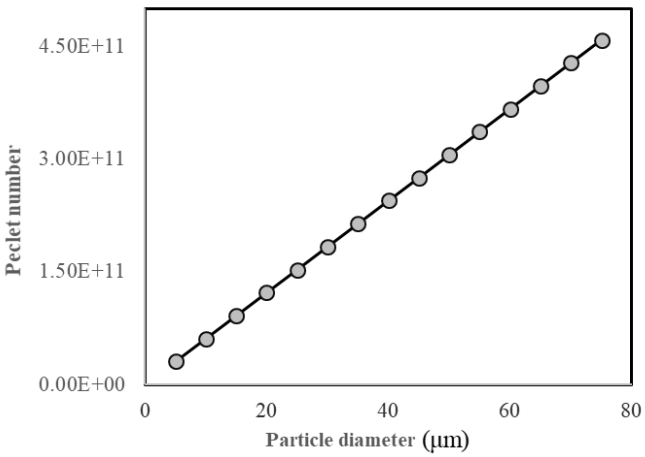

Fig. 7. Peclet number for a microparticle in a microchannel.

Figure 8 illustrates the Magnus force acting on a rigid spherical microparticle in an inertial microfluidics-based device. The fluid velocity and angular speed of the microparticle are taken as 1 m/s and 1 rad/s, respectively. The Magnus force and microparticle diameter are plotted in terms of nanonewton and micrometre, respectively. It is found that this force gradually increases when the microparticle diameter is increased from 5 to 75 micrometres. Comparing Fig. 3 and Fig. 8 indicates that the Magnus force is very small compared to the drag force in inertial microfluidics. It should be noticed that the drag force is plotted in terms of micronewton while the Magnus force is calculated in terms of nanonewton.

The influences of the microparticle size on the Saffman and wall-induced forces in an inertial microfluidics-based device are shown in Figs. 9 and 10, respectively. It is worth mentioning that the microparticle is rigid and spherical; moreover, the microchannel is a cylindrical microtube. In Fig. 10, it is assumed that the whole boundary has an influence on the microparticle. It

is observed that the particle diameter plays a crucial role in both Saffman and wall-induced forces. Both of these forces remarkably increase when the particle diameter is increased. In addition, it is found that generally, the wall-induced force in inertial microfluidics is around ten times higher than the Saffman force. However, both forces are much higher than the Magnus and diffusion forces.

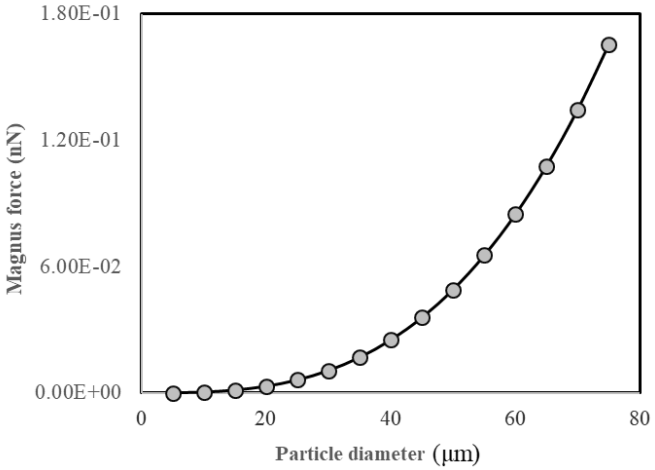

Fig. 8. Magnus force acting on a microparticle in a microchannel versus the particle diameter.

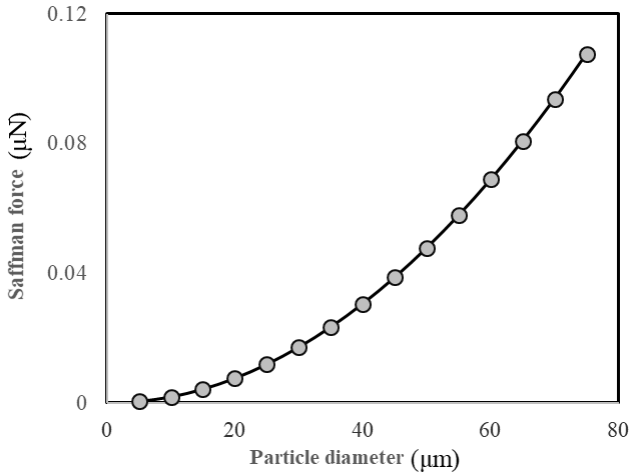

Fig. 9. Saffman force acting on a microparticle in a microchannel versus the particle diameter.

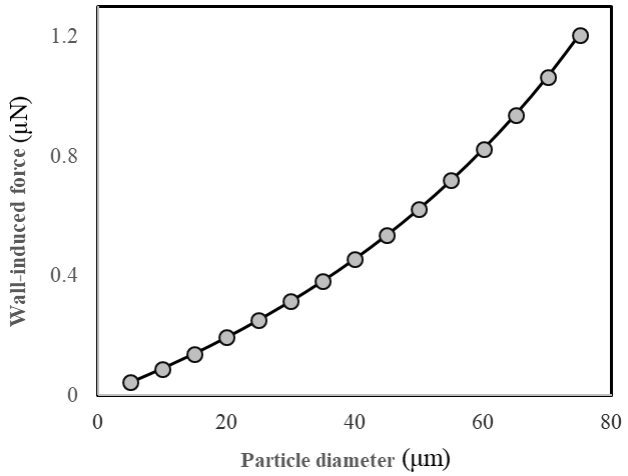

Fig. 10. Wall-induced lift force acting on a rigid spherical microparticle in a cylindrical microtube versus the particle diameter.

8. Conclusions

The dynamic behaviour of microparticles in an inertial microfluidics-based device has been investigated based on fluid mechanics. Various intrinsic forces such as drag, Magnus, Saffman, diffusion and wall-induced forces, which act on particles in the device, were theoretically formulated. In addition, explicit relations were proposed for the drag coefficient in a wide range of particle Reynolds numbers. Moreover, the diffusion coefficient and Peclet number for a spherical microparticle in the channel of the device were investigated. The influences of particle size on various forces as well as the diffusion and drag coefficients were also analysed. It was concluded that compared to drag, Saffman and wall-induced forces, forces due to the diffusion and Magnus force can be ignored. Furthermore, it was found that the drag force increases with increasing the particle diameter while the drag coefficient substantially decreases when the diameter of the particle increases. The Peclet number is very high for microparticles in an inertial microfluidics-based device, indicating that the effects of diffusion are negligible. In addition, as the size of the particle grows, both Saffman and wall-induced forces dramatically increase.

References

[1] S. Asemi, A. Farajpour, M. Mohammadi, Nonlinear vibration analysis of piezoelectric nanoelectromechanical resonators based on nonlocal elasticity theory, *Composite Structures*, Vol. 116, pp. 703-712, 2014.

[2] J. S. Bunch, A. M. Van Der Zande, S. S. Verbridge, I. W. Frank, D. M. Tanenbaum, J. M. Parpia, H. G. Craighead, P. L. McEuen, Electromechanical resonators from graphene sheets, *Science*, Vol. 315, No. 5811, pp. 490-493, 2007.

[3] W. Guo, C. Cheng, Y. Wu, Y. Jiang, J. Gao, D. Li, L. Jiang, Bio-inspired two-dimensional nanofluidic generators based on a layered graphene hydrogel membrane, *Advanced Materials*, Vol. 25, No. 42, pp. 6064-6068, 2013.

[4] M. R. Farajpour, A. Rastgoo, A. Farajpour, M. Mohammadi, Vibration of piezoelectric nanofilm-based electromechanical sensors via higher-order non-local strain gradient theory, *IET Micro & Nano Letters*, Vol. 11, No. 6, pp. 302-307, 2016.

[5] Y. Shao, J. Wang, H. Wu, J. Liu, I. A. Aksay, Y. Lin, Graphene based electrochemical sensors and biosensors: a review, *Electroanalysis: An International Journal Devoted to Fundamental and Practical Aspects of Electroanalysis*, Vol. 22, No. 10, pp. 1027-1036, 2010.

[6] M. R. Farajpour, A. R. Shahidi, A. Farajpour, Frequency behavior of ultrasmall sensors using vibrating SMA nanowire-reinforced sheets under a non-uniform biaxial preload, *Materials Research Express*, Vol. 6, pp. 065047, 2019.

[7] M. M. Adeli, A. Hadi, M. Hosseini, H. H. Gorgani, Torsional vibration of nano-cone based on nonlocal strain gradient elasticity theory, *The European Physical Journal Plus*, Vol. 132, No. 9, pp. 393, 2017.

[8] A. Daneshmehr, A. Rajabpoor, A. Hadi, Size dependent free vibration analysis of nanoplates made of functionally graded materials based on nonlocal elasticity theory with high order theories, *International Journal of Engineering Science*, Vol. 95, pp. 23-35, 2015.

[9] A. Hadi, M. Z. Nejad, M. Hosseini, Vibrations of three-dimensionally graded nanobeams, *International Journal of Engineering Science*, Vol. 128, pp. 12-23, 2018.

[10] M. Z. Nejad, A. Hadi, A. Rastgoo, Buckling analysis of arbitrary two-directional functionally graded Euler–Bernoulli nano-beams based on nonlocal elasticity theory, *International Journal of Engineering Science*, Vol. 103, pp. 1-10, 2016.

[11] S. S. Kuntaegowdanahalli, A. A. S. Bhagat, G. Kumar, I. Papautsky, Inertial microfluidics for continuous particle separation in spiral microchannels, *Lab on a Chip*, Vol. 9, No. 20, pp. 2973-2980, 2009.

[12] H. Vahabi, E. R. Rad, T. Parpaite, V. Langlois, M. R. Saeb, Biodegradable polyester thin films and coatings in the line of fire: the time of polyhydroxyalkanoate (PHA)?, *Progress in Organic Coatings*, Vol. 133, pp. 85-89, 2019.

[13] M. R. Farajpour, A. R. Shahidi, A. Farajpour, Elastic waves in fluid-conveying carbon nanotubes under magneto-hygro-mechanical loads via a two-phase local/nonlocal mixture model, *Materials Research Express*, Vol. 6, pp. 0850a8, 2019.

[14] M. Farajpour, A. Shahidi, A. Farajpour, Influences of non-uniform initial stresses on vibration of small-scale sheets reinforced by shape memory alloy nanofibers, *The European Physical Journal Plus*, Vol. 134, No. 5, pp. 218, 2019.

[15] A. Farajpour, A. Rastgoo, M. Farajpour, Nonlinear buckling analysis of magneto-electro-elastic CNT-MT hybrid nanoshells based on the nonlocal continuum mechanics, *Composite Structures*, Vol. 180, pp. 179-191, 2017.

[16] M. Farajpour, A. Shahidi, A. Farajpour, A nonlocal continuum model for the biaxial buckling analysis of composite nanoplates with shape memory alloy nanowires, *Materials Research Express*, Vol. 5, No. 3, pp. 035026, 2018.

[17] M. Farajpour, A. Shahidi, A. Hadi, A. Farajpour, Influence of initial edge displacement on the nonlinear vibration, electrical and magnetic instabilities of magneto-electro-elastic nanofilms, *Mechanics of Advanced Materials and Structures*, Vol. DOI: 10.1080/15376494.2018.1432820, 2018.

[18] M. Farajpour, A. Shahidi, F. Tabataba'i-Nasab, A. Farajpour, Vibration of initially stressed carbon nanotubes under magneto-thermal environment for nanoparticle delivery via higher-order nonlocal strain gradient theory, *The European Physical Journal Plus*, Vol. 133, No. 6, pp. 219, 2018.

[19] M. R. Farajpour, A. Shahidi, A. Farajpour, Resonant frequency tuning of nanobeams by piezoelectric nanowires under thermo-electro-magnetic field: a theoretical study, *Micro & Nano Letters*, Vol. 13, No. 11, pp. 1627-1632, 2018.

[20] M. Hosseini, M. Shishesaz, K. N. Tahan, A. Hadi, Stress analysis of rotating nano-disks of variable thickness made of functionally graded materials, *International Journal of Engineering Science*, Vol. 109, pp. 29-53, 2016.

[21] M. Z. Nejad, A. Hadi, A. Farajpour, Consistent couple-stress theory for free vibration analysis of Euler-Bernoulli nano-beams made of arbitrary bi-directional functionally graded materials, *Structural Engineering and Mechanics*, Vol. 63, No. 2, pp. 161-169, 2017.

[22] M. Hosseini, A. Hadi, A. Malekshahi, M. Shishesaz, A review of size-dependent elasticity for nanostructures, *Journal of Computational Applied Mechanics*, Vol. 49, No. 1, pp. 197-211, 2018.

[23] N. Kordani, A. Fereidoon, M. Divsalar, A. Farajpour, Forced vibration of piezoelectric nanowires based on nonlocal elasticity theory, *Journal of Computational Applied Mechanics*, Vol. 47, No. 2, pp. 137-150, 2016.

[24] E. Rohani Rad, M. R. Farajpour, Influence of taxol and CNTs on the stability analysis of protein microtubules, *Journal of Computational Applied Mechanics*, Vol. DOI: 10.22059/JCAMECH.2019.277874.369, 2019.

[25] M. Abdelgawad, A. R. Wheeler, Low-cost, rapid-prototyping of digital microfluidics devices, *Microfluidics and nanofluidics*, Vol. 4, No. 4, pp. 349, 2008.

[26] J. Zhang, S. Yan, D. Yuan, G. Alici, N.-T. Nguyen, M. E. Warkiani, W. Li, Fundamentals and applications of inertial microfluidics: A review, *Lab on a Chip*, Vol. 16, No. 1, pp. 10-34, 2016.

[27] M. E. Warkiani, B. L. Khoo, L. Wu, A. K. P. Tay, A. A. S. Bhagat, J. Han, C. T. Lim, Ultra-fast, label-free isolation of circulating tumor cells from blood using spiral microfluidics, *Nature protocols*, Vol. 11, No. 1, pp. 134, 2016.

[28] M. E. Warkiani, A. K. P. Tay, B. L. Khoo, X. Xiaofeng, J. Han, C. T. Lim, Malaria detection using inertial microfluidics, *Lab on a Chip*, Vol. 15, No. 4, pp. 1101-1109, 2015.

[29] V. Potluri, P. S. Kathiresan, H. Kandula, P. Thirumalaraju, M. K. Kanakasabapathy, S. K. S. Pavan, D. Yarravarapu, A. Soundararajan, K. Baskar, R. Gupta, An inexpensive smartphone-based device for point-of-care ovulation testing, *Lab on a Chip*, Vol. 19, No. 1, pp. 59-67, 2019.

[30] A. J. Chung, A Minireview on Inertial Microfluidics Fundamentals: Inertial Particle Focusing and Secondary Flow, *BioChip Journal*, Vol. 13, No. 1, pp. 53-63, 2019.

[31] D. Di Carlo, Inertial microfluidics, *Lab on a Chip*, Vol. 9, No. 21, pp. 3038-3046, 2009.

[32] A. Kommajosula, D. Stoecklein, D. Di Carlo, B. Ganapathysubramanian, Shape-design for stabilizing micro-particles in inertial microfluidic flows, *arXiv preprint arXiv:1902.05935*, 2019.

[33] N. Liu, C. Petchakup, H. M. Tay, K. H. H. Li, H. W. Hou, *Spiral Inertial Microfluidics for Cell Separation and Biomedical Applications*, in: *Applications of Microfluidic Systems in Biology and Medicine*, Eds., pp. 99-150: Springer, 2019.

[34] J. M. Coulson, J. F. Richardson, J. R. Backhurst, J. H. Harker, 1991, *Particle technology and separation processes*, Pergamon Press,

[35] S. R. Asemi, A. Farajpour, Vibration characteristics of double-piezoelectric-nanoplate-systems, *Micro & Nano Letters*, Vol. 9, No. 4, pp. 280-285, 2014.

[36] S. R. Asemi, A. Farajpour, M. Borghei, A. H. Hassani, Thermal effects on the stability of circular graphene sheets via nonlocal continuum mechanics, *Latin American Journal of Solids and Structures*, Vol. 11, No. 4, pp. 704-724, 2014.

[37] A. Farajpour, A. Rastgoo, Influence of carbon nanotubes on the buckling of microtubule bundles in viscoelastic cytoplasm using nonlocal strain gradient theory, *Results in physics*, Vol. 7, pp. 1367-1375, 2017.

[38] A. Farajpour, A. Rastgoo, M. Mohammadi, Vibration, buckling and smart control of microtubules using piezoelectric nanoshells under electric voltage in thermal environment, *Physica B: Condensed Matter*, Vol. 509, pp. 100-114, 2017.

[39] M. Farajpour, A. Shahidi, A. Farajpour, Influence of shear preload on wave propagation in small-scale plates with nanofibers, *Structural Engineering and Mechanics* Vol. 70, No. 4, pp. 407-420 2019.

[40] M. Goodarzi, M. Mohammadi, A. Farajpour, M. Khooran, Investigation of the effect of pre-stressed on vibration frequency of rectangular nanoplate based on a visco-Pasternak foundation, *Journal of Solid Mechanics*, Vol. 6, pp. 98-121, 2014.

[41] S. R. Asemi, M. Mohammadi, A. Farajpour, A study on the nonlinear stability of orthotropic single-layered graphene sheet based on nonlocal elasticity theory, *Latin American*

Journal of Solids and Structures, Vol. 11, No. 9, pp. 1515-1540, 2014.

[42] M. Safarabadi, M. Mohammadi, A. Farajpour, M. Goodarzi, Effect of surface energy on the vibration analysis of rotating nanobeam, *Journal of Solid Mechanics*, Vol. 7, No. 3, pp. 299-311, 2015.

[43] R. M. Mazo, 2002, *Brownian motion: fluctuations, dynamics, and applications*, Oxford University Press on Demand,

[44] R. Clift, J. R. Grace, M. E. Weber, 2005, *Bubbles, drops, and particles*, Courier Corporation,

[45] E. Michaelides, 2006, *Particles, bubbles & drops: their motion, heat and mass transfer*, World Scientific,

[46] P. Saffman, The lift on a small sphere in a slow shear flow, *Journal of fluid mechanics*, Vol. 22, No. 2, pp. 385-400, 1965.

[47] H. Brenner, The slow motion of a sphere through a viscous fluid towards a plane surface, *Chemical engineering science*, Vol. 16, No. 3-4, pp. 242-251, 1961.

[48] R. Cox, S. Hsu, The lateral migration of solid particles in a laminar flow near a plane, *International Journal of Multiphase Flow*, Vol. 3, No. 3, pp. 201-222, 1977.